Chapter 5

Efficiency Boosting for PV Systems- MPPT Intelligent Control Based

Farhat Maissa and Sbita Lassâad

Additional information is available at the end of the chapter

http://dx.doi.org/10.5772/59399

1. Introduction

Nowadays renewable energy techniques for power production are mature and reliable. The photovoltaic (PV) energy is the most promising source of energy since it is pollution free and abundantly available everywhere in the world. PV energy is especially beneficial in remote sites like deserts or rural zones where the difficulties to transport fuel and the lack of energy grid lines make the use of conventional resources impossble. Pumping water in these sites is a vital task that requires a feasible source of energy to supply power to the electrical elements of the pumping structure.

This work analyses the control of a stand-alone PV pumping system. The success of a PV application depends on the effectiveness of the power electronic devices to efficiently operate the photovoltaic generator (PVG) even under variable climatic conditions The big need is to extract the maximum of power from the PVG at any climatic input levels. Therefore, the reliability of the MPPT controller is of paramount importance in successful PV pumping applications.

The MPPT control is a challenge, because the PVG sunshine energy input flux may change at any time. In fact, the PV system is considered as a non-linear complex one. For these reasons, the design of an appropriate setup controller is difficult to build. In the literature, numerous MPPT methods have been developed, among them: The hill climbing, incremental conductance and the P&O [1]. These algorithms consist of introducing a crisp values positive or negative (decrease or increase) all around the actual PVG operating point. From the previous power point position, the trajectory of the new one helps the algorithm to decide on the command output value. This algorithm may fail to act as an accurate MPPT because of the used crisp value (step size) that is mainly fixed by trial and tests running.

The intelligent techniques have recently attracted the interest of engineers due to several facts: as Self-Optimization fast convergence and simplicity of combination with classical extremum seeking [2], [3]. In this work the interest was focus on applying these techniques on the photovoltaic fields. In this work, the control strategy is described and tested in the context of a highly dynamic input.

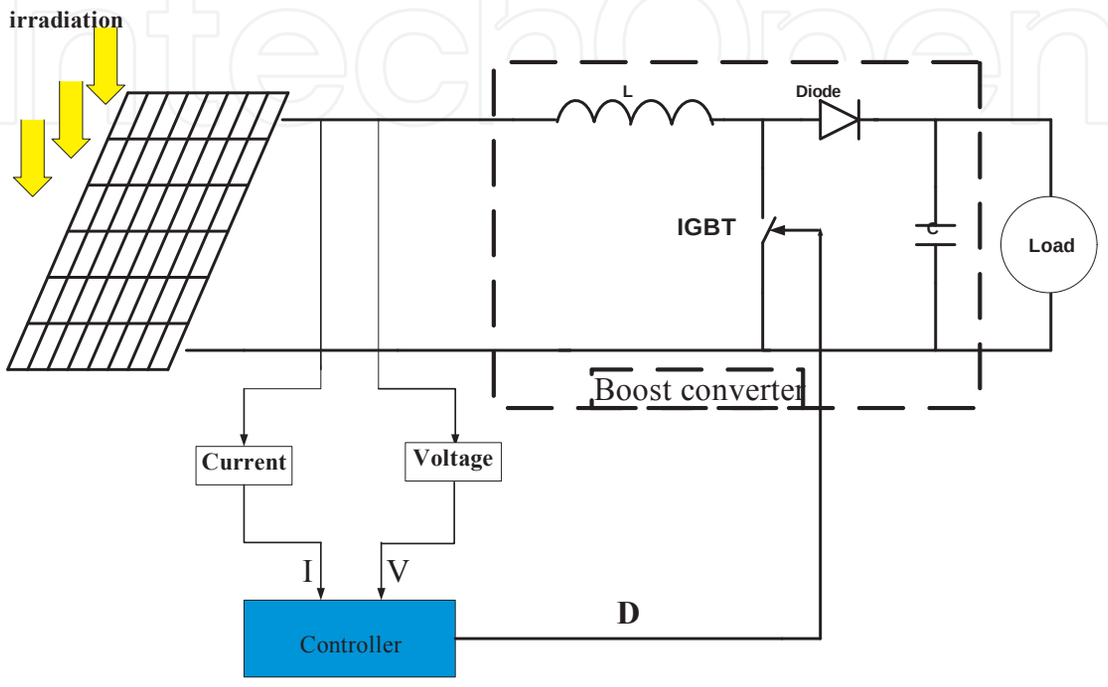

Figure 1. Synoptic diagram of PV system

2. Modeling of photovoltaic system

One can substitute a PV cell to an equivalent electric circuit which includes a power supply, resistors and a diode as shown in figure 2.

The power source generate a current called an I_{ph} current, this last depends on the irradiation amount. [1], [4], [5].

Up on the node law;

$$I_c = I_{ph} - I_d - I_{sh} \tag{1}$$

The current I_{ph} can be evaluated as:

http://dx.doi.org/10.5772/59399

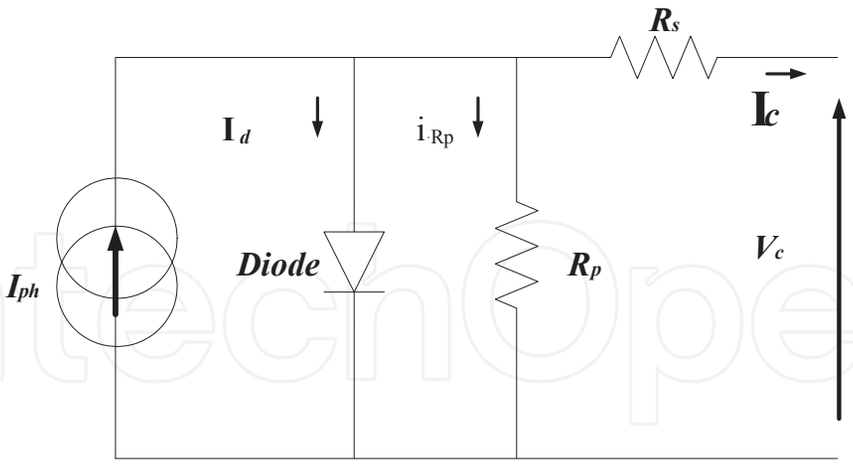

Figure 2. Simplified PV Cell Equivalent Circuit

$$I_{ph} = \frac{G}{G_{ref}}\left(I_{sc\_ref} + K_{SCT}\left(T_c - T_{c\_ref}\right)\right) \tag{2}$$

And the cell current is

$$I_c = I_{ph} - I_{rs}\left(\exp(\frac{q}{n\beta T_c}\left(V_c + R_s I_c\right) - 1\right) - \frac{\left(V_c + R_s I_c\right)}{R_p} \tag{3}$$

With I_{rs} reverse saturation current is:

$$I_{rs} = I_{rs\_ref}\left(\frac{T_c}{T_{c\_ref}}\right)^3 \exp\left[\frac{qE_g}{n\beta}\left(\frac{1}{T_c} - \frac{1}{T_{c\_ref}}\right)\right] \tag{4}$$

The modeling of a PV Array depending on Ns and Np is then deduced as [5]:

$$\begin{cases} I_p = N_p I_c \\ V_p = n_s N_s V_c \\ R_s = \frac{n_s N_s}{N_p} R_s \\ R_p = \frac{n_s N_s}{N_p} R_p \end{cases} \tag{5}$$

Finally the I_p panel current can be given by

$$I_p = N_p I_{ph} - N_p I_{rs}\left(\exp\frac{q}{n\beta T_c}\left(\frac{V_p}{n_s N_s}+\frac{R_s I_p}{N_p}\right)-1\right)-\frac{N_p}{R_p}\left(\frac{V_p}{n_s N_s}+\frac{R_s I_p}{N_p}\right) \quad (6)$$

The cartelistic I-V in various irradiation and temperature is shown in figure 3

It is clear to find the three specific operating points in figure 3(a) [5].

- zone of voltage: characterized by an open circuit voltage V_{OC}.,
- zone of current: characterized by a short – circuit current I_{SC},
- Zone of maximum of power (P_{max}.) It is necessary to operate the PV at the third zone to extract the maximum power from the PVG.

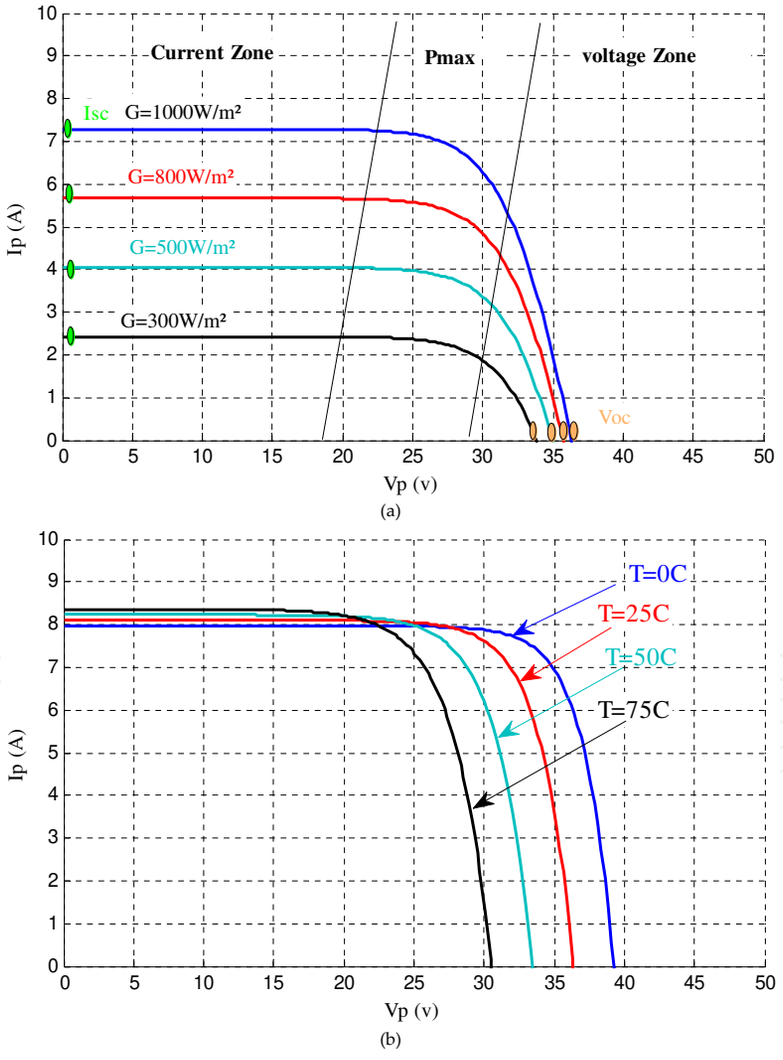

Figure 3. I-V characteristics of the PVG for variable: (a) irradiation at a constant temperature of 25°C, (b) temperature at a constant irradiation (1000W/m²)

http://dx.doi.org/10.5772/59399

3. Boost converter

DC-DC converters are electronic devices used whenever is needed to change DC electrical power efficiently from one voltage level to another. A DC-DC converter is an adapter controlling the load power through a regulated duty cycle. In order to step up the voltage, the operation consists of switching an IGBT (Figure 4) at a high commutation frequency, with output voltage control by varying the switching duty cycle (D) [6] and [7].

$$V_{in} = (1 - D)V_o \tag{7}$$

Where D is the actual duty cycle.

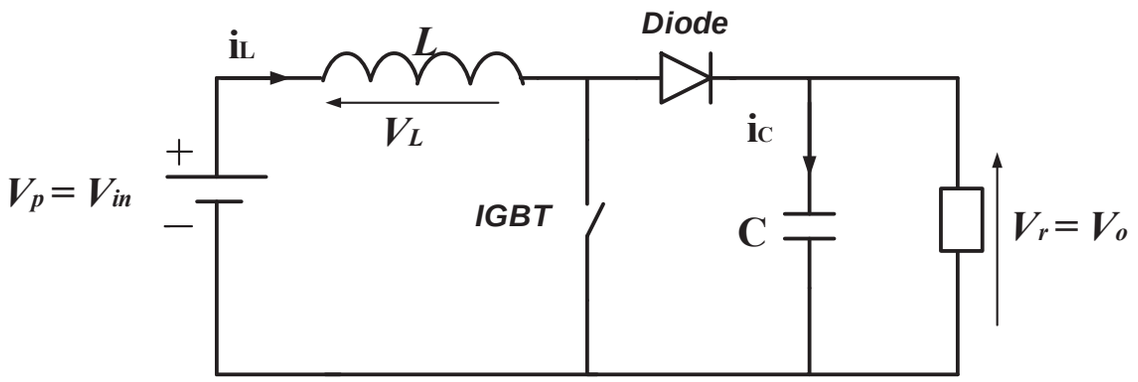

Figure 4. Circuit diagram of the used Boost converter

4. P&O algorithm principle

Due to its simplicity, P&O algorithm is the most popular one [5]. The principle of this scheme is to generate a crisp value by acting (decrease /increase) on the duty cycle actual command (D) and then observe the output power reaction. If the actual power P(k) is lower than the previous one, then the acting direction is inversed otherwise it is maintained [8], [9].

When dP/ dV>0, the voltage is increased, this yields to

D (K)= D (K)+ΔD, (ΔD: crisp value)

When dP/ dV< 0, the voltage is decreased through

D (k) = D (k −1) −ΔD.

The ΔD crisp value is chosen by trial and tests in simulation. The P&O diagram is shown in figure 5:

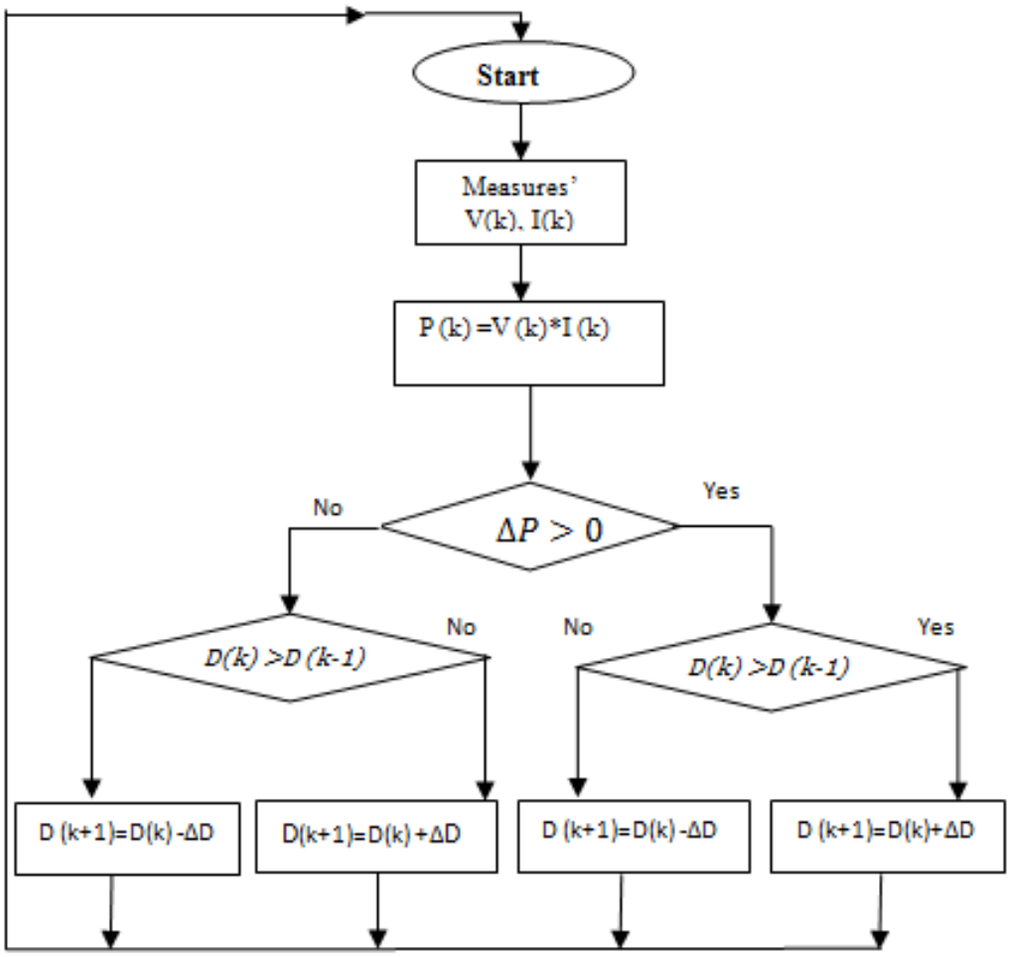

Figure 5. P&O Algorithm structure

If the crisp value ΔD is very big or very small then we may lose information as shown in figure 6. Despite the P&O algorithm is easy to implement it has mainly the following problems [9]:

- the PV system always operates in an oscillating mode.
- the operation of PV system may fail to track the maximum power point.

The ΔD crisp value is chosen by trial and tests in simulation. The P&O diagram is illustrated in fig. 5.

5. Intelligent Artificial MPPT Control technics

In this section, the most investigated Intelligent Artificial control techniques are considered. In particular, The artificial neuronal networks (ANN), the Fuzzy Logic control (FLC), and the adaptive neuro-fuzzy inference system (ANFIS) as the best one that combines the FLC and ANN advantages.

http://dx.doi.org/10.5772/59399

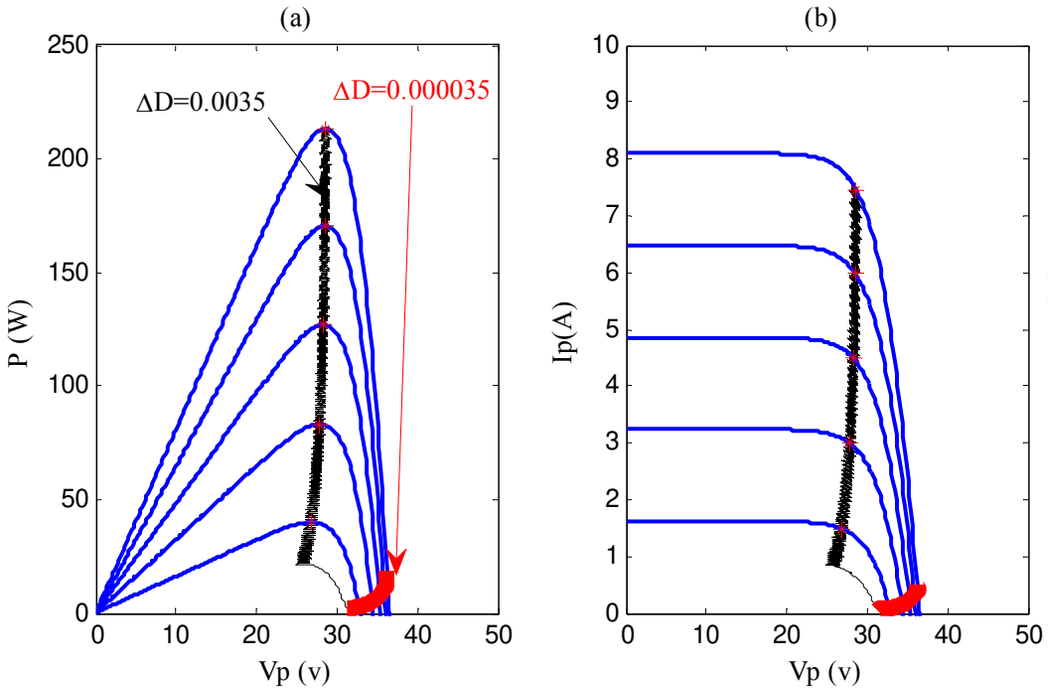

Figure 6. P-V, I-V curves and the MPPT-P&O for ΔD: (a) 0.0035 ET (b) 0.000035

5.1. ANN

Artificial Neural network (ANN) method have been employed successfully in solving problems with a high degree of complexness in various fields and applications including pattern recognition, identification vision, prediction,control systems and classification, [10]. Now the ANN can be used in order to solve a lot of problems that are difficult for conventional computers or even for human beings. ANNs, overcome the limitations of the conventional approaches, and present a solution by extracting the desired information directly from the experimental data. The fundamental element of a neural-network is neurons. The method is based on neurons receiving input from other neurons, after that the ANN combines them in a non-linear operation and then generate outputs as a final result. [11].

Artificial neural network was used as a controller to track the maximum power point by commanding the boost converter. Effectively the MPPT artificial neural controller is composed in general by a three layers, first; an input, then hidden and finally an output layer [12],[13], This connection is characterized respectively by weights, w^{I} and w^{o}, like presented in figure 7.

The mathematical expressions define the relation between the input and the output signals are given in equation 8, 9 and 10.

- The output layer :

$$D^{na}(k) = f\left(\sum_{j=1}^{nc} w^{o}{}_{i}(k)\, y_{i}(k)\right) \tag{8}$$

- The output hidden layer:

$$y_i(k) = f\left(S_j(k)\right) = \frac{1}{1+\exp(-S_j(k))} \tag{9}$$

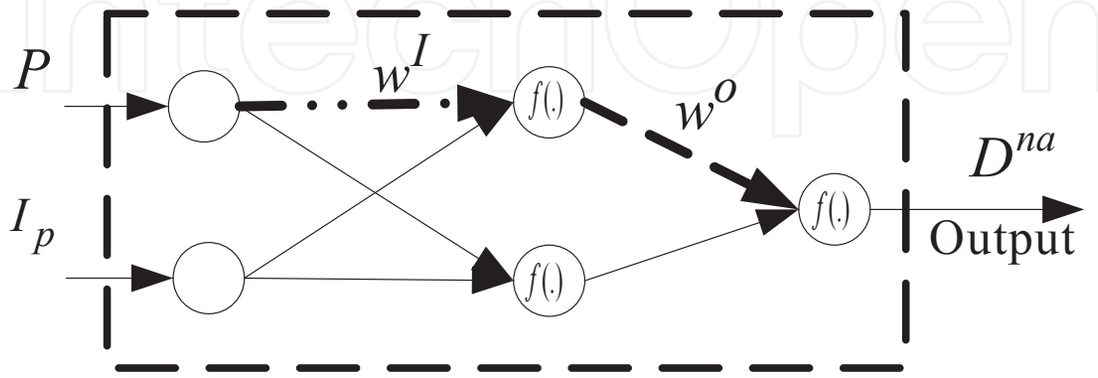

Figure 7. Structure of an artificial neural network

- The hidden layer:

$$H_j(k) = \sum_{i=1}^{ne} w_{j,i}^I(k)\, x_j(k) \tag{10}$$

qWhere '*nc*' represent the neurons number in the hidden and '*ne* ' the output layer. The data vector x_i represents the input signals that are given in equation 11 [11].

$$x_i = \left[D^*(k) \quad P(k-1) \quad I_P(k-1) \right]^T \tag{11}$$

in the ANN_MPPT Controller, an activation function defines each neuron. The sigmoid function has been chosen for this work.

To achieve the required input/output relationship, an adjustment of weights between the output layer and the hidden layer, and the input layer and the hidden layer is required. for the weights updating ;the back propagation algorithm is used, by minimized an error function defined in equation 12 [11].

$$E_{na}\ (k) = \frac{1}{2}\left[D^*(k) - D^{na}(k) \right]^2 = \frac{1}{2} e_{na}^2(k) \tag{12}$$

Where $D^*(k)$ is the desired output, $E_{na}(k)$ is the accrued output, and $e_{na}(k)$ represent the error between the desired and accrued output

The updating of weights is calculated by using the gradient method [11].

$$w_{i,1}^{o}(k+1) = w_{i,1}^{o}(K) + \Delta w_{i,1}^{o}(K) = w_{i,1}^{o}(K) - \eta^{o}(K)\frac{\partial E_{na}(K)}{\partial w_{i,1}^{o}(K)} \tag{13}$$

$$w_{j,i}^{I}(k+1) = w_{j,i}^{I}(K) + \Delta w_{j,i}^{I}(K) = w_{j,i}^{I}(K) - \eta^{I}(K)\frac{\partial E_{na}(K)}{\partial w_{j,i}^{I}(K)} \tag{14}$$

Where $\eta_{na}{}^{o}$, $\eta_{na}{}^{I}$ are respectively the ANN learning rates for the hidden and the output layer.

The quantity $\frac{\partial E_{na}(K)}{\partial w^{I}(K)}$ and $\frac{\partial E_{na}(K)}{\partial w^{o}(K)}$ are respectively calculated by the equation 15 and 16.

$$\frac{\partial E_{na}(K)}{\partial w^{I}(K)} = -e_{na}(k)\,y_i(k) \tag{15}$$

$$\frac{\partial E_{na}(K)}{\partial w^{o}(K)} = -e_{na}(k)\,w^{o}{}_{i,1}(k)\,x_j(k) \tag{16}$$

Figure 8 is the windows given by the Matlab at the starting of learning, where the neural model performance, the structure, the learning function, and the maximum training patterns, are given. It's clear that the ANN performance is good as shown in figure 9 witch present an error of learning equal to 10E-8 the neural architecture used for this model is [11].:

- 2 neurons in the input layer,
- 2 neurons in the first next hidden layer, and 4 neurons in the second one
- 1 neuron in the output layer
- the learning rates is 0.01

The training pattern is 100 epoch.

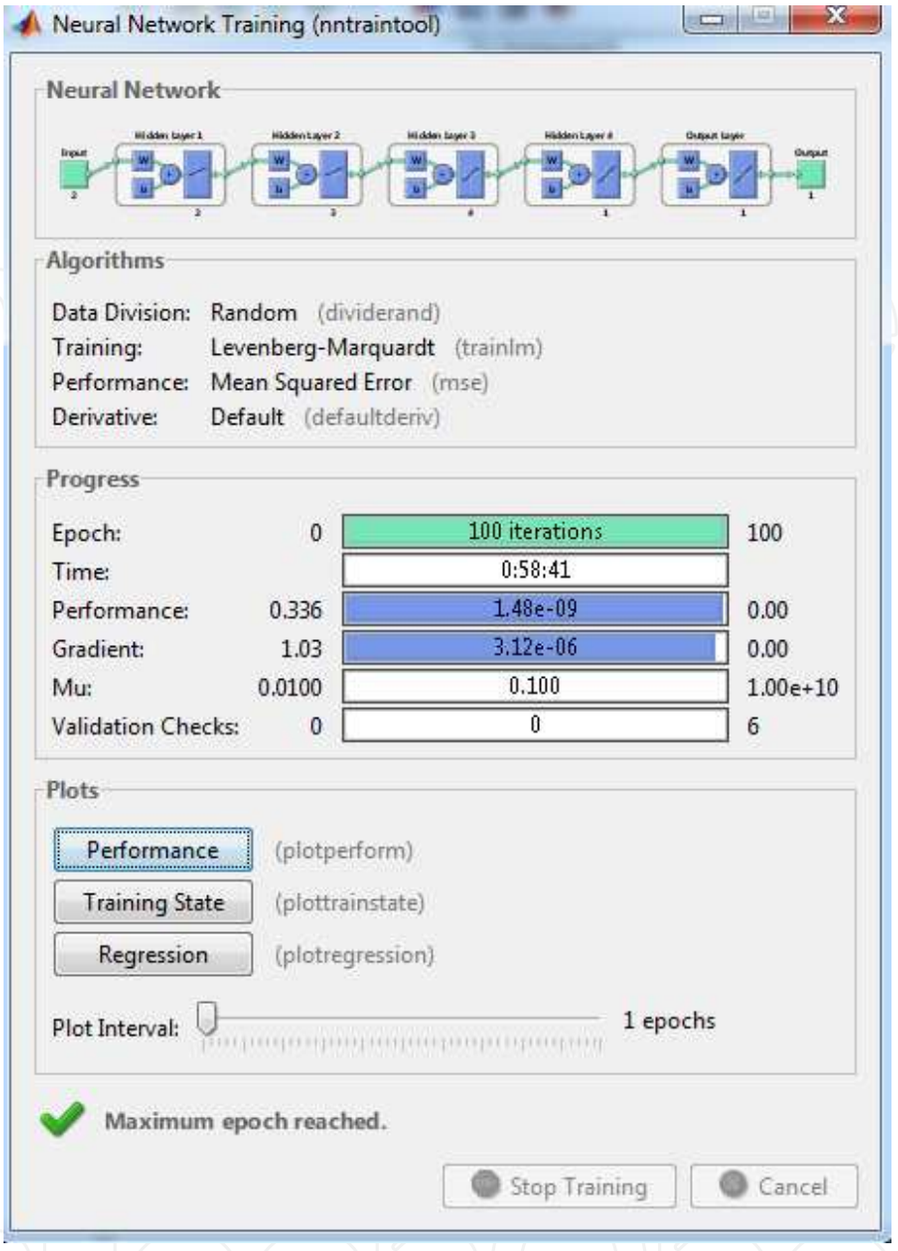

Figure 8. Neuronal network training

For simulation work, the Data Base has been created by using the *Ip*-and *Vp* then calculating the optimal duty cycle eq (21).

$$P_{in} = P_{out} \tag{17}$$

$$V_p \times I_p = V_r \times I_r \tag{18}$$

Utilizing equation (7)

http://dx.doi.org/10.5772/59399

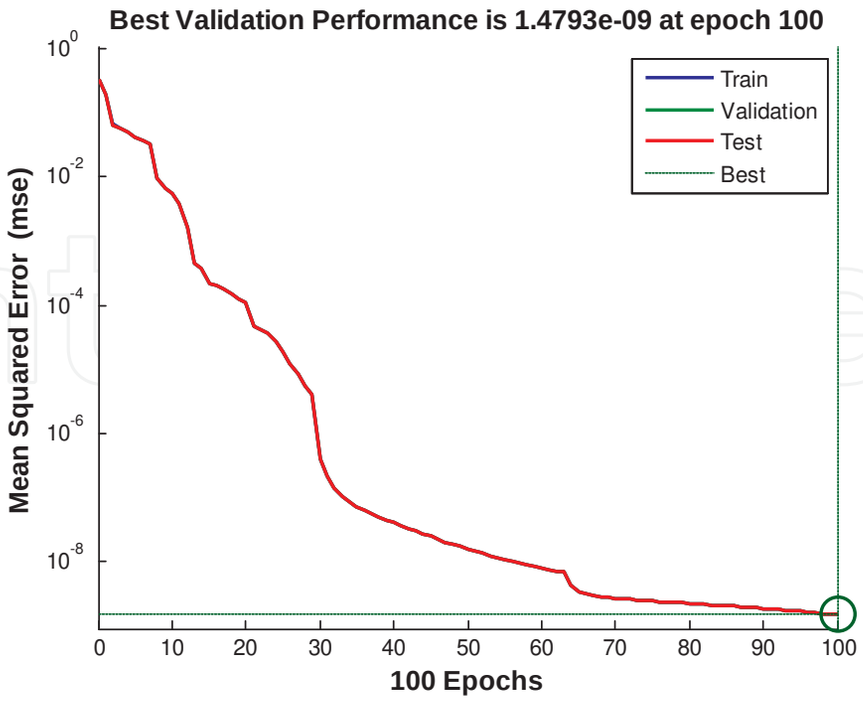

Figure 9. Validation performance

$$V_p \times I_p = \frac{V_r^2}{R} \tag{19}$$

$$V_p \times I_p = \frac{V_p^2}{(1-D)^2 R} \tag{20}$$

$$D = 1 - \sqrt{\frac{V_p}{R \times I_p}} \tag{21}$$

The result obtained using the $D_{opt} = 1 - \sqrt{\frac{V_{opt}}{R \times I_{opt}}}$ will be used as reference for the t other controllers and will be named as $\text{MPPT}_{\text{ideal with}}$ V_{opt} and I_{opt} are respectively the voltage and current of the Maximum power point

5.2. Fuzzy-logic control (FLC)

FLC is a way that mimics the human capability of judgment and reasoning [12]. A typical FLC based approach is composed by three modules [13]. fuzzification, Inference, defuzzification to made a closed-loop system that uses the process of fuzzification to generate fuzzy inputs to

an inference engine processes the fuzzy sets using a library of IF-THEN. The defuzzification is the inverse process, used in a FLC control system in order to generate the create step size real values.

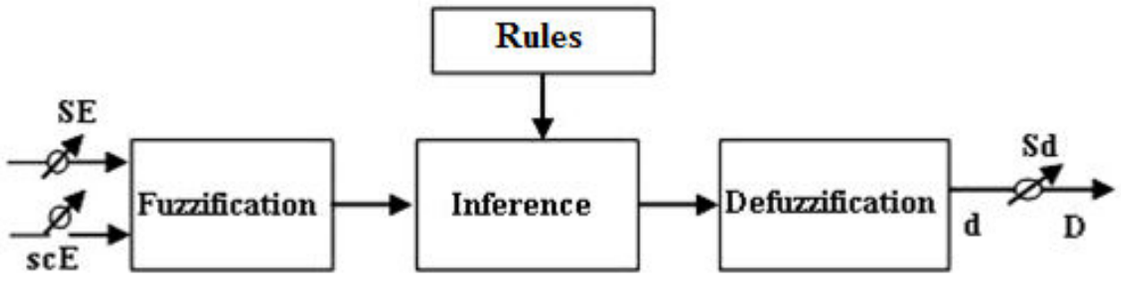

Figure 10. FLC controller structure

To adjust the controller input/output, SE, SCE and Sd gains are introduced. The controller crisp value (ΔD) is the output and the two variables E and CE represent respectively the error and it's derivate as the controller inputs [14].

$$\begin{cases} E(k) = \dfrac{P_{ph}(k) - P_{ph}(k-1)}{V_{ph}(k) - V_{ph}(k-1)} \\ CE(k) = E(k) - E(k-1) \end{cases} \tag{22}$$

With $P_{ph}(k)$ is the PV generator instantaneous power.

The input E (k) shows if the load operating point at the instant k is located on the left or on the right of the maximum power point on the PV characteristic, while the input CE (k) expresses the moving direction of this point.

The fuzzy inference is carried out by using Mamdani method, Table 1, and the defuzzification uses the center of gravity to compute the controller output [14]:

$$\Delta D = \frac{\sum_{j=1}^{n} \mu(\Delta D_j).\Delta D_j}{\sum_{j=1}^{n} \mu(\Delta D_j)} \tag{23}$$

The control rules are indicated in Table 1 with E and CE as inputs and ΔD as output. The corresponding variables member ship functions are given in Figure11.

The membership functions of E, CE and ΔD are depicted in figure 11:

http://dx.doi.org/10.5772/59399

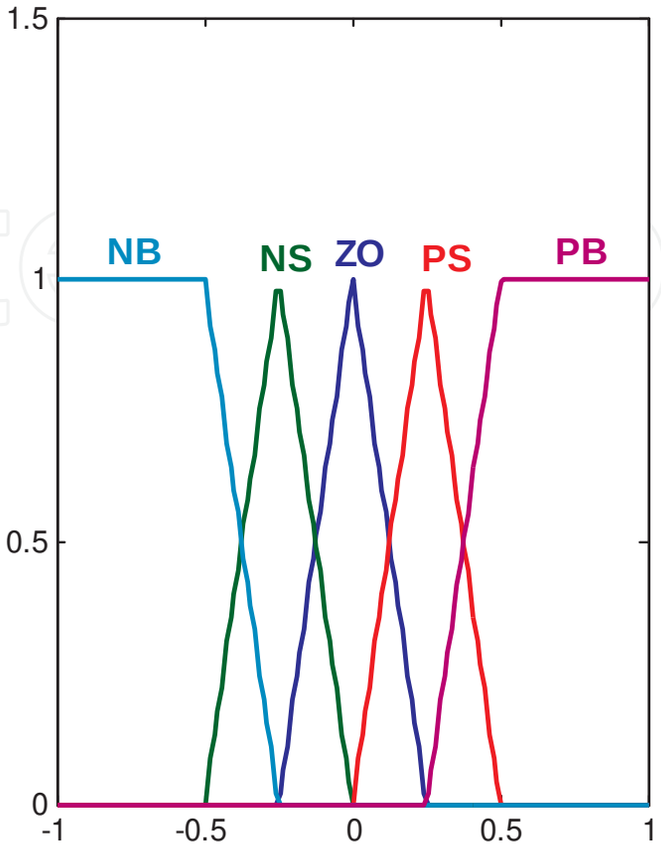

Figure 11. Membership functions of E, CE and D

	CE				
E	*NB*	*NS*	ZO	*PS*	*PB*
NB	ZO	ZO	*PB*	*PB*	*PB*
NS	ZO	ZO	*PS*	*PS*	*PS*
Z0	*PS*	ZO	ZO	ZO	*NS*
PS	*NS*	*NS*	*NS*	ZO	ZO
PB	*NB*	*NB*	*NB*	ZO	ZO

Table 1. Fuuzzy logic controller Rules.

5.3. An adaptive neuro-fuzzy inference contol

Neuro-fuzzy technique is combining the ANN learning methods and the fuzzy inference system (FIS) [15], [16], [17]. In general the FIS structure consists of three important components:

and the rule base one, for rule fuzzy selection [18]; a database, which defines the fuzzy rules MF and a decision generator, that bring up the inference procedure to finally generate an output as shown in Figure 12. The FLC concepts are based on knowledge from expert and in the other hand the neural network models are using a data base. Moreover, neuro-fuzzy approach seems covenant and suitable if both advantages of the tow method are combined. The neuro-fuzzy controller is the called, in this work adaptive network (ANFIS). The structure of the system is an adaptive network running as a first-order Sugeno fuzzy inference system. The hybrid ANFIS learning rule, combine the back-propagation gradient-descent first and second a least-squares algorithm for identification and optimization of the the Sugeno first order system. The the ANFIS working process is simplified by an equivalent ANFIS architecture with two rules are given in Figure 13 [4], [16], [18].

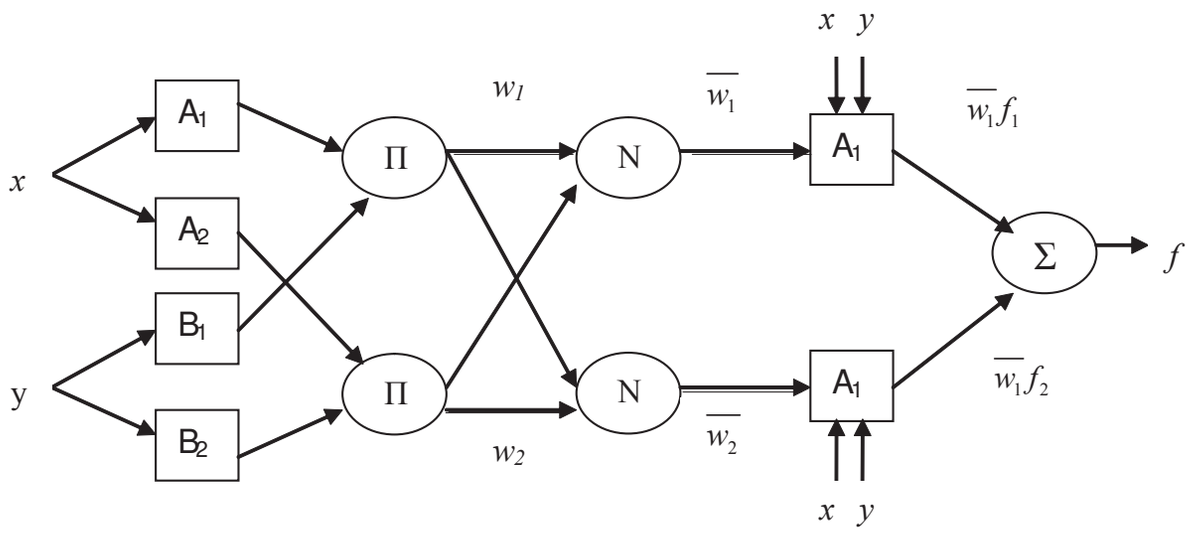

Figure 12. Architecture of The ANFIS model Sugeno's fuzzy inference method

The given architecture has five layers and every node in a layer has a similar function. The two fuzzy rules, in which outputs are dressed as linear combinations of their inputs, are [4]:

$$\text{Rule 1}: \text{ if x is } A_1 \text{ and y is } B_1 \text{ then } f_1 := p_1x + q_1x + r_1 \tag{24}$$

$$\text{Rule 2}: \text{if x is } A_2 \text{and y is } B_2 \text{ then } f_2 := p_2x + q_2x + r_2 \tag{25}$$

Layer 1: consists of adaptive nodes that generate membership grades of linguistic labels based upon premise signals, using any appropriate parameterized membership function such as the generalized bell function given by [4]:

$$O_{1i} = \mu_{A_i}(x) = \frac{1}{1+\left|\frac{x-c_i}{a_i}\right|^{2b_i}} \tag{26}$$

Where output O1,i is the output of the ith node in the first layer, x is the input to node i, Ai is a linguistic label ("small," "large," etc.) from fuzzy set A =(A1, A2, B1, B2,) associated with he node, and {ai, bi, ci} is the premise parameter set used to adjust the shape of the membership function [4]:.

Layer 2: are fixed nodes designated Π, which represent the firing strength of each rule. The output of each node is the fuzzy AND (product or MIN) of all the input signals [4]::

$$o_{2,i} = w_i = \mu_{Ai}(x)\mu_{Bi}(y) \quad \text{i=1, 2} \tag{27}$$

Layer 3: The outputs are the normalized firing strengths. Each node is a fixed rule labeled N. The output of the ith node is the ratio of the ith rule's firing strength to the sum of all the rules firing strengths [4]::

$$o_{3,i} = \overline{w_i} = \frac{w_i}{w_1 + w_2} \tag{28}$$

Layer 4: the equation gives the rule outputs is:

$$o_{4,i} = \overline{w_i} f_i = \overline{w_i}(p_i x + q_i y + r_i) \tag{29}$$

With $\overline{w_i}$ is the firing strength that is normalized from the layer number 3, p_i, q_i, r_i are the node set parameters.

Layer 5: the ANFIS output is given by:

$$o_{5,i} = \sum_i \overline{w_i} f_i = \frac{\sum_i w_i f_i}{\sum_i w_i} \tag{30}$$

The ANFIS controller developed in this section includes ' Ip ' and ' P ' as inputs and 'D' as output which represent respectively, the PV current, the PV-Power and the converter duty cycle ratio. The input variables allow the ANFIS to generate the converter command. This last is applied to the converter, in order to ensure the adaptation of the power provided by PVG. This controller yields to an automatic fuzzy rules generation based on the Sugeno inference model. The equivalent neural structure of the proposed ANFIS is given in figure 13, figure 14 show the MPPT-ANFIS validation and errors curves.

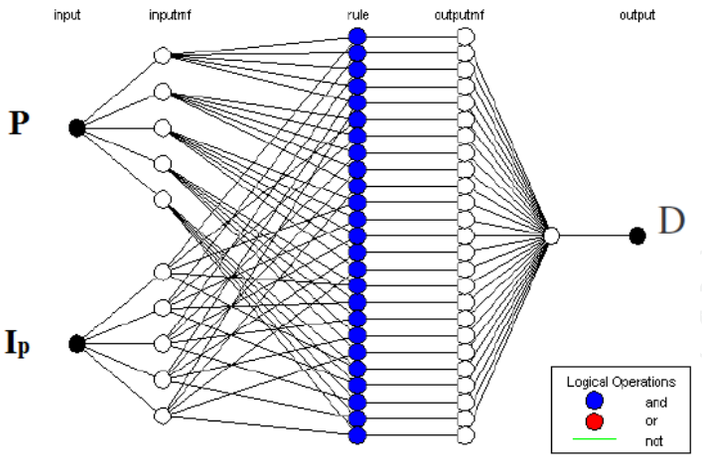

Figure 13. Structure of proposed neuronal model

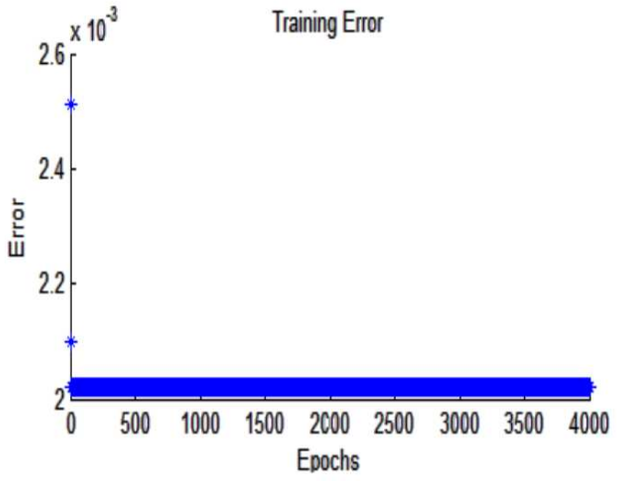

(a)

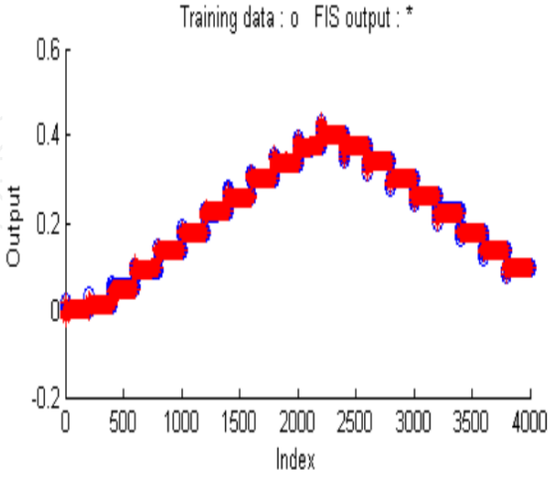

(b)

Figure 14. MPPT-ANFIS validation and errors curves

http://dx.doi.org/10.5772/59399

6. Simulation results

In this section the performance of MPPT controller; Fuzzy, Neuronal, ANFIS will be distingue by the comparison between them and $MPPT_{ideal}$, he signal corresponding to the ideal MPPT present the reference used to compare the performances of various MPPT controllers

6.1. FLC

The figure 15 shows that the Fuzzy flow th $MPPT_{ideal}$, the FLC controllers ensure a good maximum power tracking. Nevertheless, the fuzzy regulator is oscillating around the MPP zone and is not powerful especially on weak irradiation level.

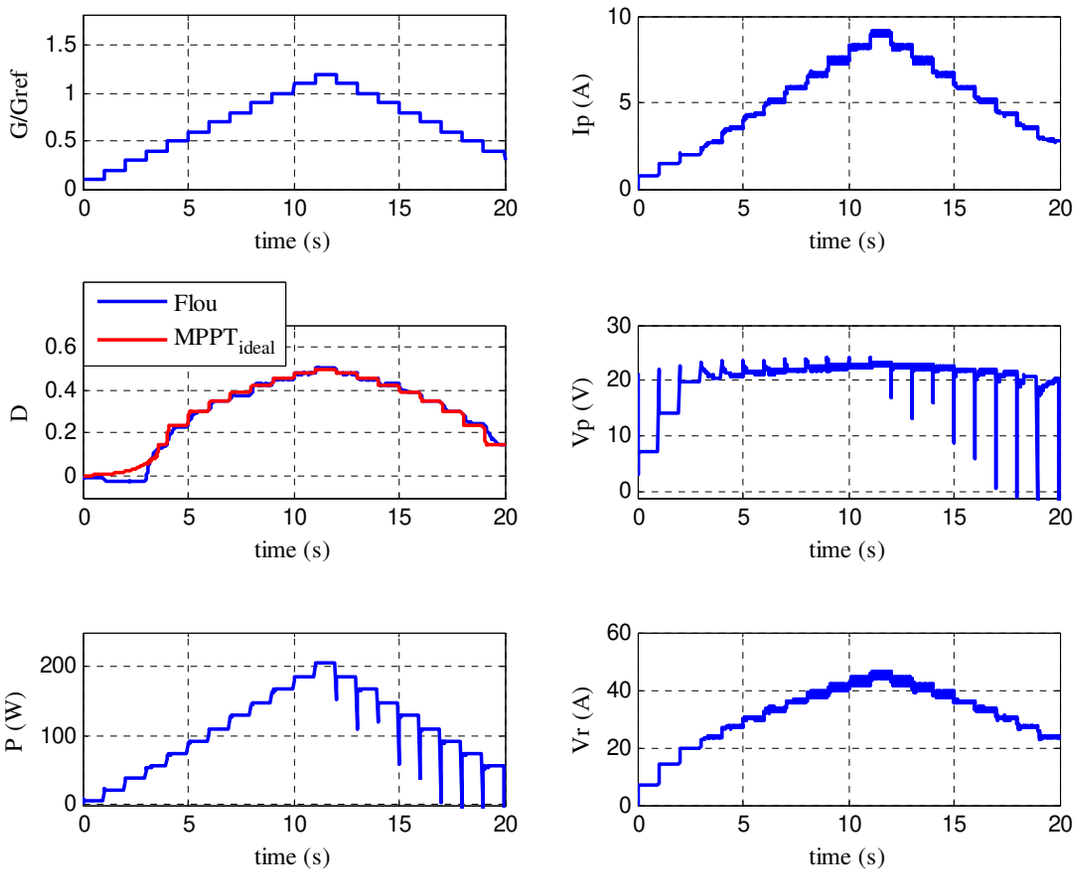

Figure 15. Irradiation, duty cycle, power, Power (FUZZY/$MPPT_{ideal}$), PV current, PV voltage, converter voltage in different values of irradiation (100 to 1200W/m², 25°C)

6.2. Neuronal network

The acquired sizes I_P and P are the input. The output of the controller is the duty cyclic D commanding an MLI block of the controller. The figure 16 contains the data base adopted for the training. This base corresponds to the MPPT ideal.

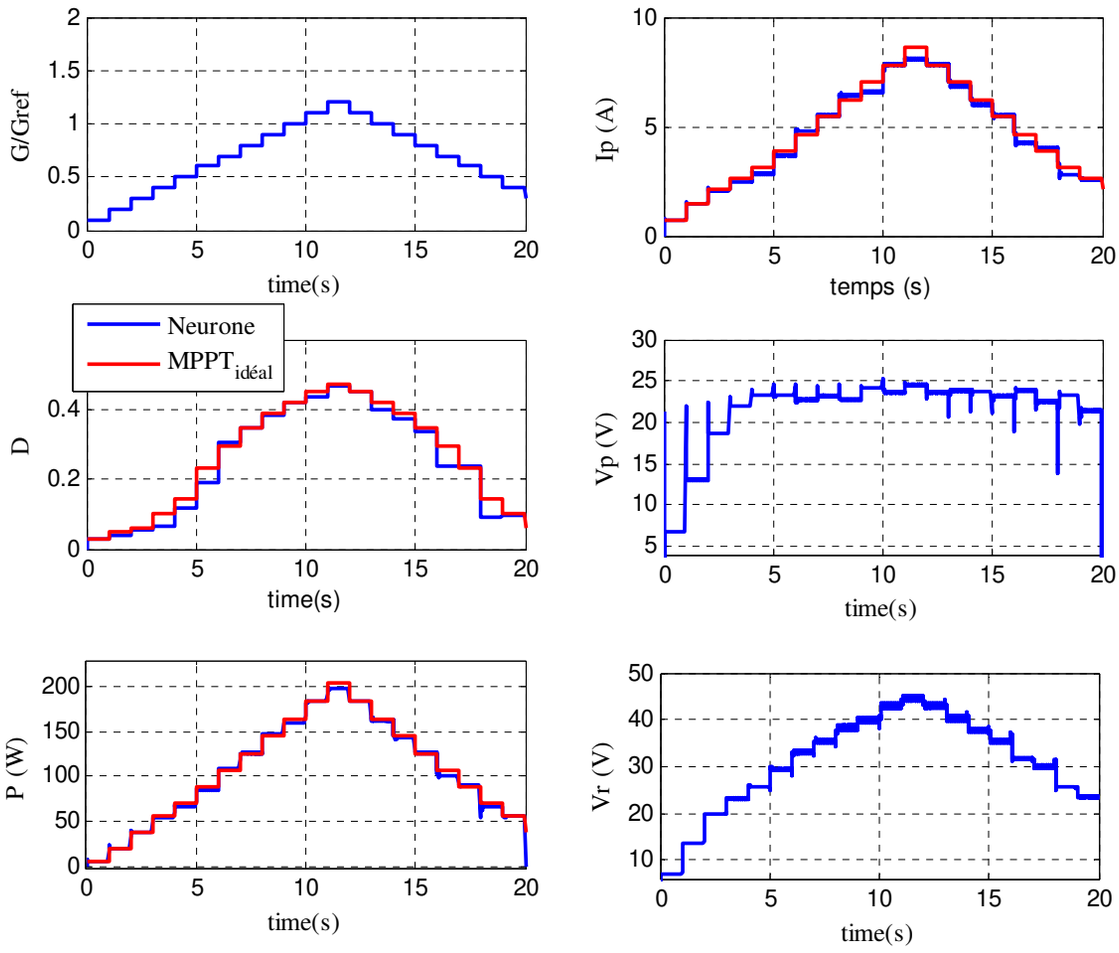

Figure 16. Irradiation, duty cycle, power, Power (Neuron/ $MPPT_{ideal}$), PV current, PV voltage, converter voltage in different values of irradiation (100 to 1200W/m², 25°C)

The figure 16 show well that controller MPPT ANN presents a mediocre performances with respect to the request of the incidental system with precipice irradiation variation. The time and the training memory capacity as well as the heaviness of a significant data base form one huge flexibility handicaps. To overcome these problems, we propose in the following section the algorithm combining the FLC and RNA.

6.3. ANFIS

The acquired sizes I_P and P are the input. The duty cyclic D is the output ordering the MLI block of Boost converter. Figure 17 contains the data base adopted for the training of the ANFIS. This base corresponds to ideal MPPT (MPPT ideal).

6.4. Comparative study

The ANFIS-MPPT Controller ensured the compensation of a reliable tracking on the low values of irradiation as shown in figure 17. The figure 18 confirms this improvement of the tracking

http://dx.doi.org/10.5772/59399

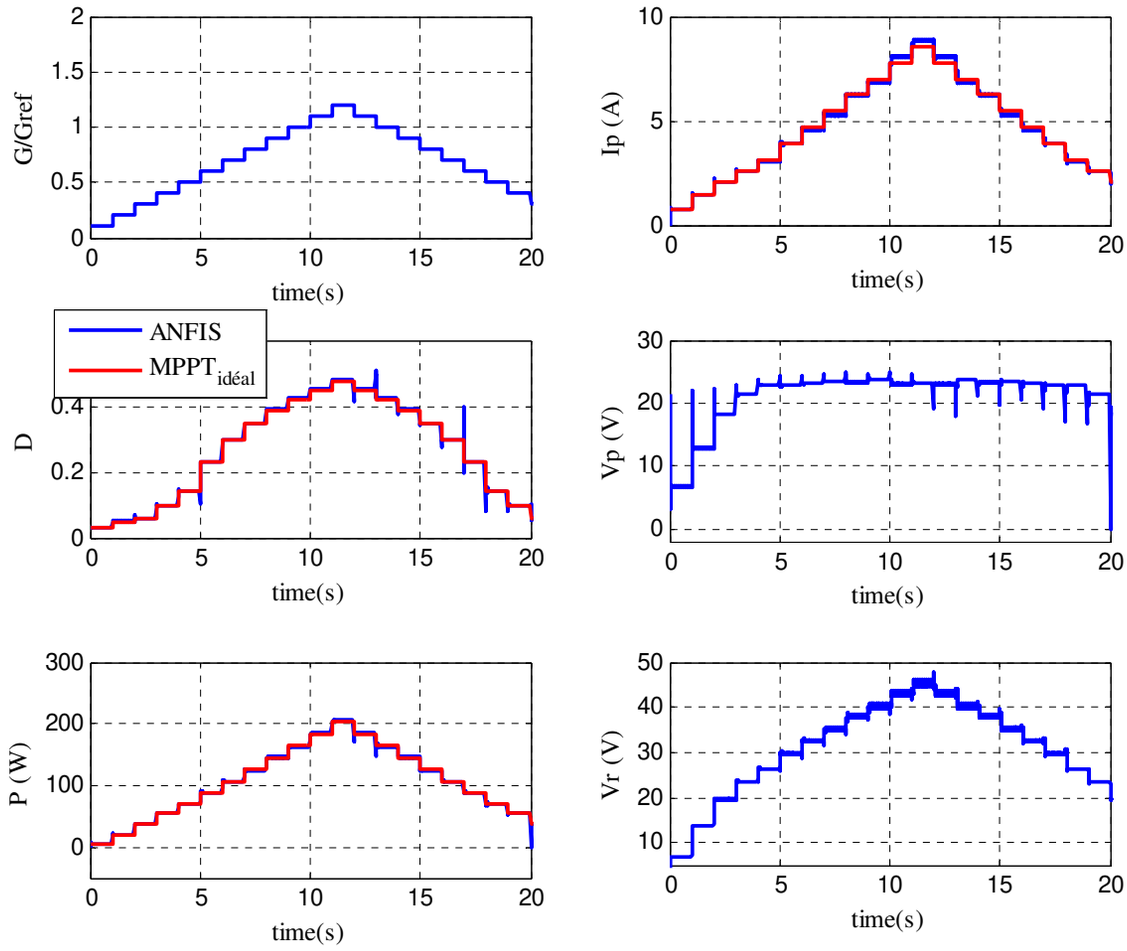

Figure 17. Irradiation, duty cycle, power, Power ratio(ANFIS/MPPT$_{ideal}$), PV current, PV voltage, converter voltage in different values of irradiation (100 to 1200W/m², 25°C)

in term of speed, increasing the step response and decreasing of error. Comparing performance put in evidence that the ANFIS precedes the RNA and the Fuzzy logic on MPPT action.

Figure 19 allows compare the different methods (P&O, Neuron, Fuzzy, ANFIS and MPPT $_{ideal}$) and this for a PV system coupled to a resistive load under a constant temperature and an irradiation (G=1000W / m², T=25C°)

The figure 18 illustrates the dynamic responses of the duty cycle and of the power of the GPV for a step of incidental irradiation of 1000W/m² and a temperature of 25°C. It is to be announced that the fuzzy controller presents a great oscillation beyond and an assailant mode to 0.6 seconds and a static error. The ANFIS and the P&O have the same response time. The RNA and for its parallel structure, justifies well the response time relatively instantaneous. The P&O and the RNA present the same static error which is larger than the fuzzy logic controller. The ANFIS MPPT is presented relatively as the most powerful controller with a static error near to zero. The figure 19 gives the plan of phase of the duty cycle according to the tension of the GPV. It is it should be noted that controller ANFIS-MPPT converges exactly towards the ideal MPPT with good performances superiors to the others.

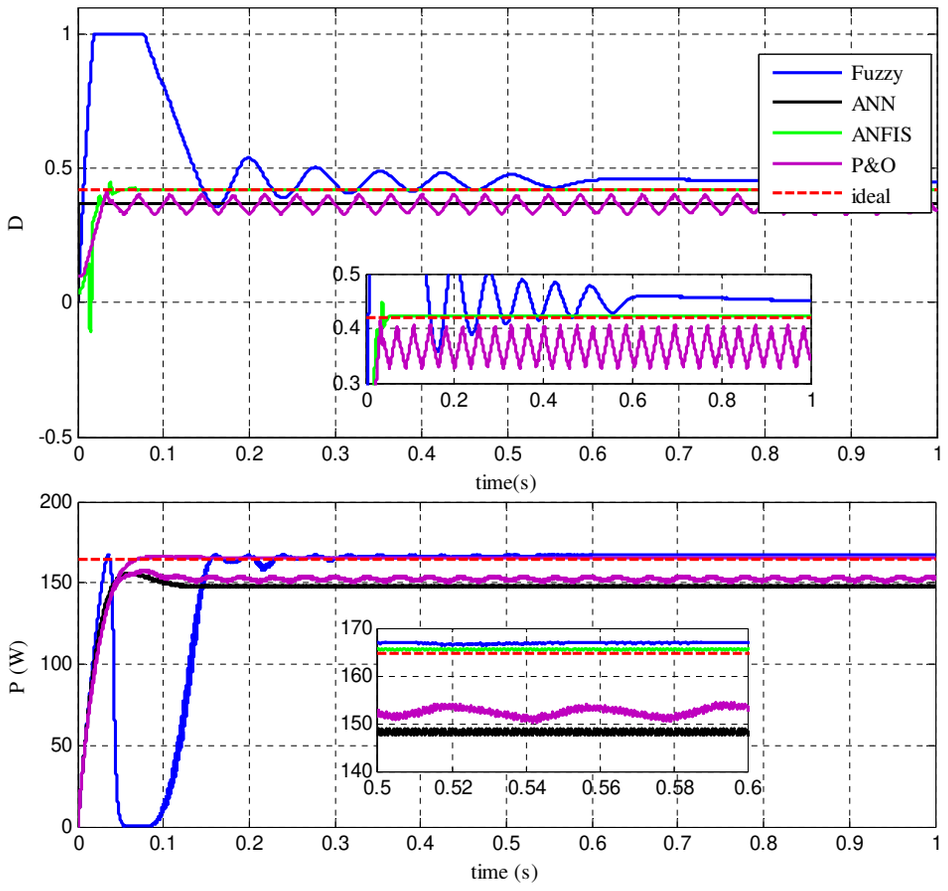

Figure 18. Fuzzy, Neuronal, Anfis and P&O duty cycle and power

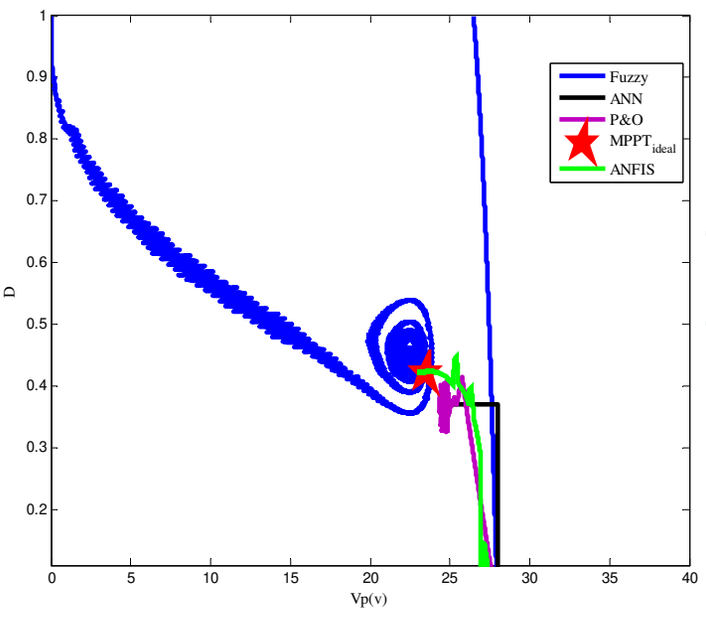

Figure 19. Fuzzy, Neuronal, Anfis and P&O performance

7. Application: Water pumping

7.1. Dc motor model

The mathematical relation that describes the dynamic model of a DC motor is given by [19]:

$$L_a \frac{dI_a}{dt} = U_a - R_a I_a - K_t \omega \tag{31}$$

$$j \frac{d\omega}{dt} = T_{em} - T_l - f\,\omega \tag{32}$$

With, L_a, Kt, V_a and I_a are armature resistance, armature inductance, back emf constant (also motor torque constant), armature voltage and current, f is constant viscous friction coefficient and J the inertia Moment. In the mechanical equation (32) T_{em} and T_L are the motor and the load (pump) torque, respectively [20].

7.2. Modeling of DC Water Pump

Recently, photovoltaic pumps use attracts more and more attention. For a positive displacement pump, the water flow of this type is depending on the drive moto shaft speed.

The piston of the pump uses the volume variations caused by the piston displacement in a cavity. The displacements in a different produce an aspiration or repression phase's dependence on the direction.

The pump piston moves in a first direction, the liquid is compressed: the induction valve is closing and the repression valve will be open. And then the operation will be reversed when the pump piston moves the second direction. This type of pump has the advantage of dry operation. However, the flow generated by this pump is limited. The model of the positive displacement pump load torque with is [21].

$$T_L = K_1 \cdot \omega + K_2 \tag{33}$$

The mathematical model that connects the pump water flow rate to the water column 'h' and power P and is: [22].

$$P(Q,h) = a(h)Q^3 + b(h)Q^2 + c(h)Q + d(h) \tag{34}$$

$$\begin{cases} a(h) = a_0 + a_1 h^1 + a_2 h^2 + a_3 h^3 \\ b(h) = b_0 + b_1 h^1 + b_2 h^2 + b_3 h^3 \\ c(h) = c_0 + c_1 h^1 + c_2 h^2 + c_3 h^3 \\ d(h) = d_0 + d_1 h^1 + d_2 h^2 + d_3 h^3 \end{cases} \tag{35}$$

Figure 19 shows the characteristics of the power according to the flow rate (P=f (Q)). They are dressed according to various heights of the water columns as given by equations 34 and 35, [4].

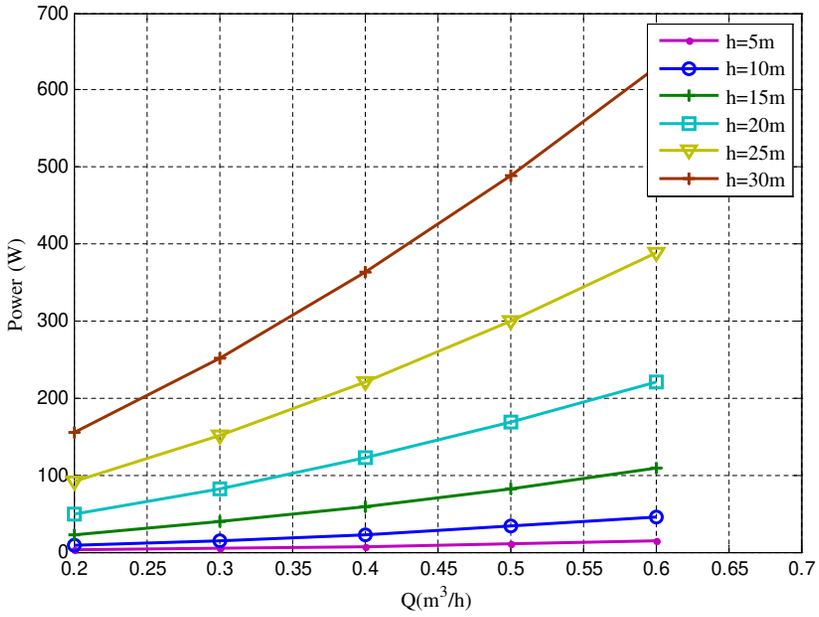

Figure 20. Pump characteristic.

From figure 19 it is easily to deduce that for a water height of 20 m, eq. 12 yields to the pumped water flow rate [11].

$$Flow = \frac{0,6}{220} P \tag{36}$$

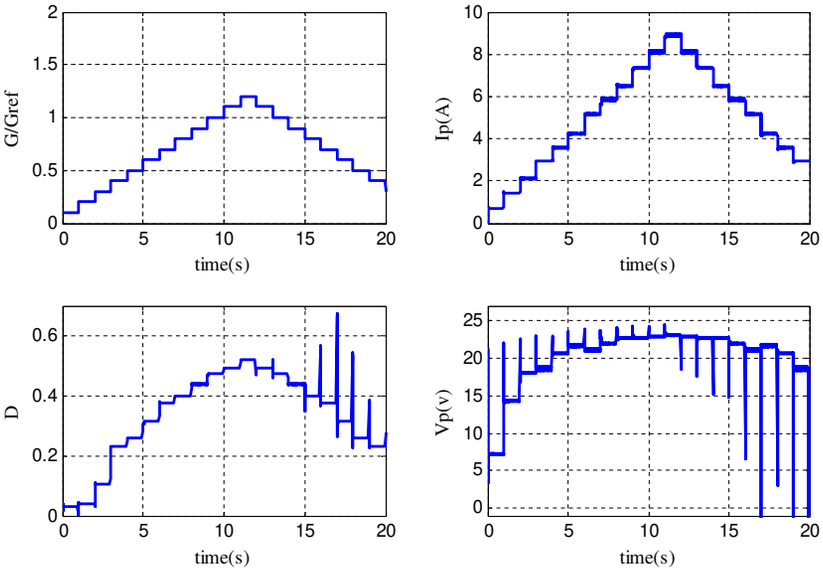

Figure 21. Irradiation, duty cycle, power, PV current, PV voltage

http://dx.doi.org/10.5772/59399

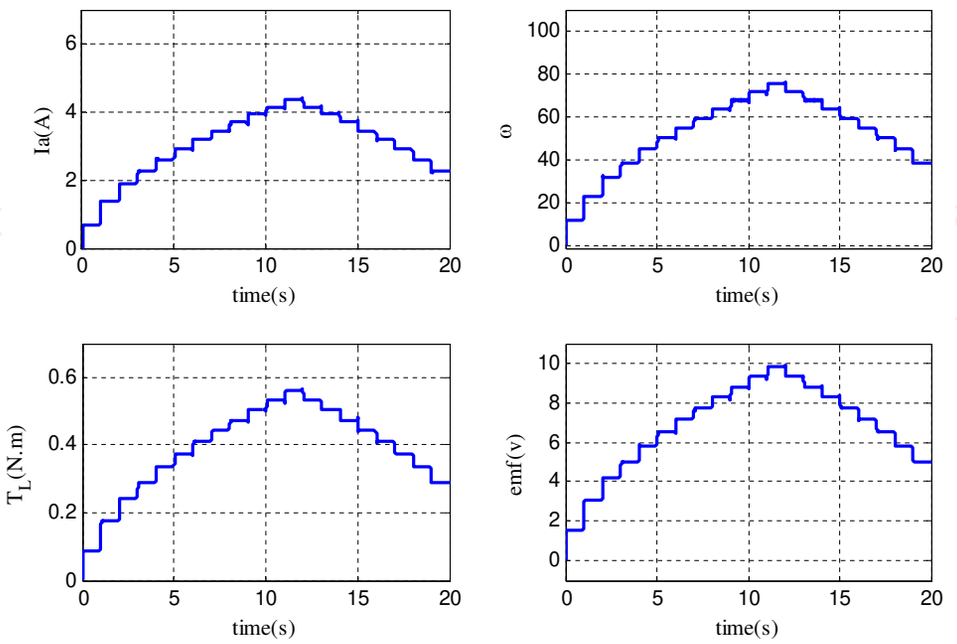

Figure 22. Motor behavouron a temprature of(25°C and various insolation

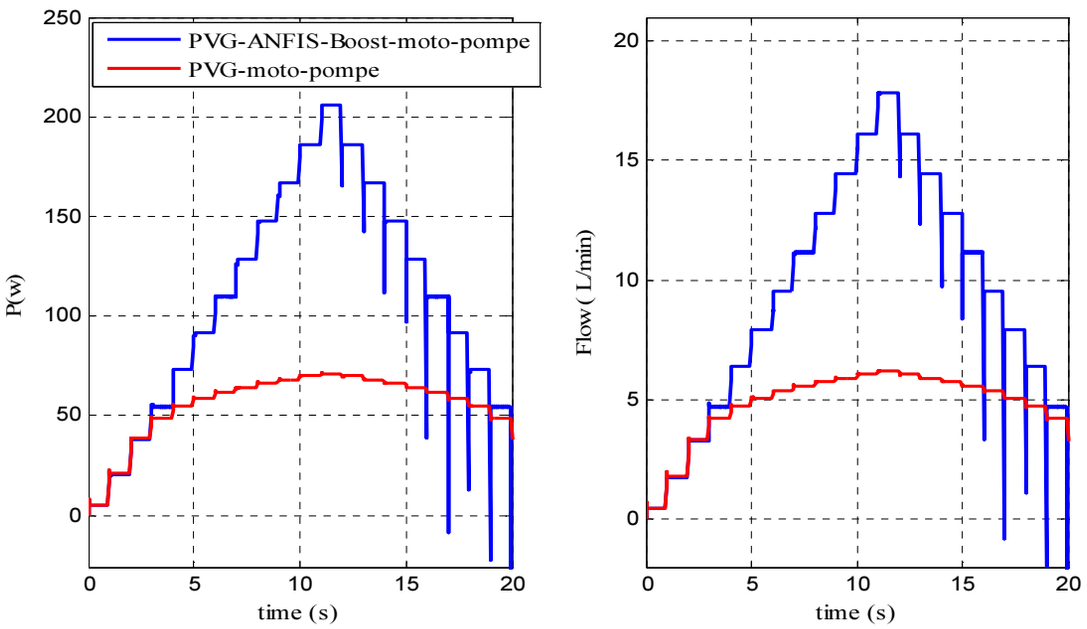

Figure 23. Power and Flow of PV pumping system with and without MPPT controller.

The MPPT ANFIS controller improves the PVG performances as clearly seen in PVG outputs tracking curves. The obtained results confirm the benefit in water flow rate is improved.

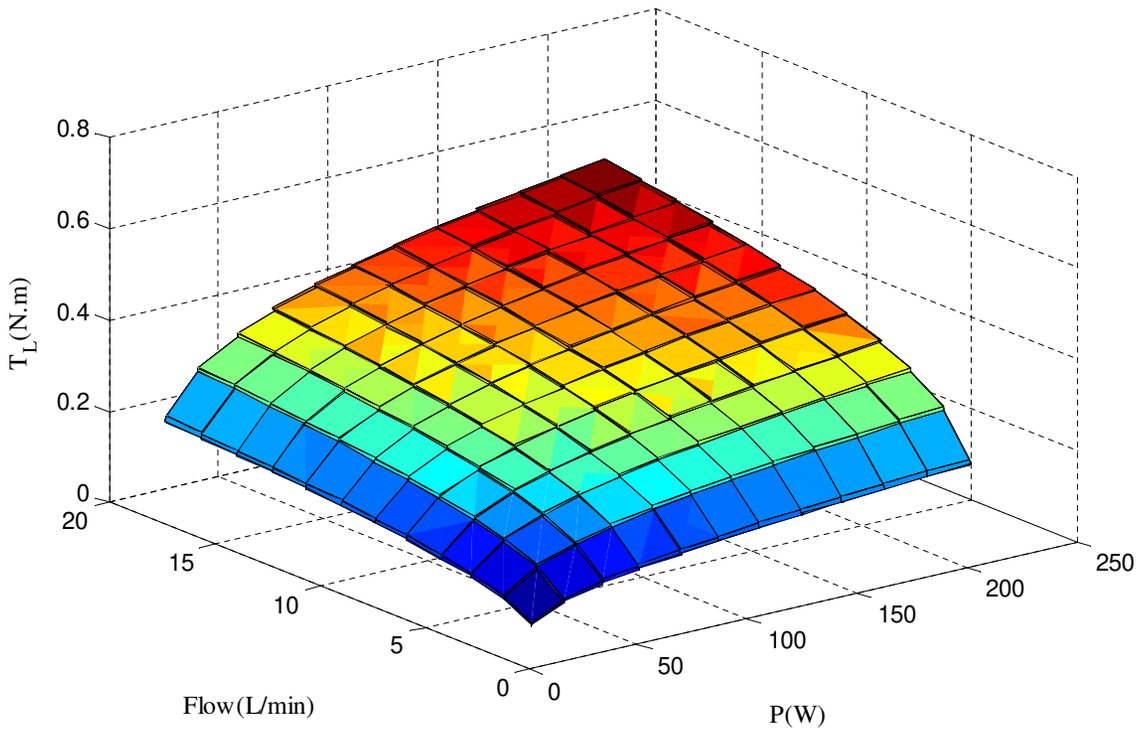

Figure 24. 3D surface of the flow power and load torque.

8. Conclusion

In this work a modeling study of the PV pumping system components is presented. Moreover in order to improve PV system performance, different maximum power point controller was studied and investigated. The system behavior incorporating the P&O, Fuzzy, ANN and neuro fuzzy were investigated and compared based on an extensive simulation work. Finally the Maximum Power Point tracking of PV pumping system is ensured by using an ANFIS controller. Performed simulation tests for the complete system lead to two main conclusions. The proposed PV system performances are highly boosted and the pumping flow rate benefit is going up to three times more [4].

Symbols

G:	Global insulation (W /m²)
Gref :	Reference insulation (W /m2)
I p:	Cell output current
Vp:	Cell output voltage
I :	Light-generated current source (A)

Rs:	cell series resistance (Ω)
Rp	Cell parallel resistance (Ω)
n:	Solar ideal factor
Irs :	Reverse diode saturation current(A)
KSCT:	Short circuit current temperature coefficient (A/°K)
Tc :	Cell junction temperature (°C)
Tc_ref :	Reference cell temperature(°C)
β :	Boltzmann constant (1.38e-23)
Eg:	Band gap energy (ev)
ns	Number of series cells.
D	duty cycle

Author details

Farhat Maissa and Sbita Lassâad*

*Address all correspondence to: lassaadsbita@yahoo.fr

Research Unit of Photovoltaic, Wind and Geothermal Systems, National Engineering School of Gabes, University of Gabes, Rue Omar Ibn-Elkhattab, Zrig, Gabès, Tunisia

References

[1] T. Esram, P. L. Chapman, Comparison of Photovoltaic Array Maximum Power Point Tracking Techniques. IEEE transactions on energy conversion, vol.22, 2007.

[2] D. Nikhitha, J.N.C. Sekhar, Modeling and Simulation of IM Drive Performance Using PI, ANN and FLC, International Conference on IT Convergence and Security (ICITCS), 2013.

[3] L.A. Torres-Salomao, J. Anzurez-Marin, Adaptive Neuro-Fuzzy Inference System Control for a Two Tanks Hydraulic System model, IEEE International Autumn Meeting on Power, Electronics and Computing (ROPEC),pp.1-5, 2013.

[4] M.farhat, L.Sbita, Advanced ANFIS-MPPT Control Algorithm for Sunshine Photovoltaic Pumping Systems, The First International Conference on Renewable Energies and VEhicular Technology, Hammamet, pp. 167- 172, from 26 to 28 March 2012.

[5] M. Farhat, A. fleh, L. Sbita., Influence of photovoltaic DC bus voltage on the high speed PMSM drive, 38th Annual Conference of the IEEE Industrial Electronics Society, 25-28 October, Montreal, Quebec, Canada, 2012.

[6] S.Hamidreza Mohades Kasaei, S. Mohammad reza Mohades Kasaei, S.Alireza Mohades Kasaei, Design and Implementation Solenoid Based Kicking Mechanism for Soccer Robot Applied in Robocup-MSL, International Journal of Advanced Robotic Systems, Vol. 7, no. 4, pp.73-80,2010.

[7] M, Zalani Daud,A, Mohamed, M. A. Hannan, An Optimal Control Strategy for DC Bus Voltage Regulation in Photovoltaic System with Battery Energy Storage The Scientific World Journal, Article ID 271087, 16 pages, 2014.

[8] S. Abouda,, F. Nollet, N. Essounbouli, A.Chaari,Y. Koubaa., Design, simulation and voltage control of standalone photovoltaic system based MPPT: Application to a pumping system, International Journal of Renewable Energy Research, vol. 3, pp. 538-549, 2013.

[9] M. farhat, L. Sbita, ANFIS controlled solar pumping system, i-manager's Journal on Electronics Engineering, Vol. 2, no. 2, march-march 2011.

[10] M. Farhat, A. Flah, L. Sbita, Photovoltaic Maximum Power Point Tracking Based on ANN Control, International Review on Modelling and Simulations (IREMOS), Vol 7, No 3, 2014.

[11] A.Flah, M.Farhat, L. Sbita, A Robust PMSM Speed Control using an Artificial and a Recurrent Neural Network, International Journal of Research and Reviews in Computer Science (IJRRCS),Vol. 2, no. 4,pp. 1023- 1028, 2011.

[12] Trishan.E, Patrick L. C, Comparison of Photovoltaic Array Maximum Power Point Tracking, Techniques, IEEE Trans. on Energy conversion, vol.22,no.2,pp. 439-449, 2007.

[13] A. Mellit, A. Kalogirou, "ANFIS-based modelling for photovoltaic power supply system: A case study, Renewable Energy: 36, pp. 250-258, 2011.

[14] Chokri. B. S, Mohamed. O, Comparison of Fuzzy Logic And Neural Network In Maximum Power Point Tracker For PV Systems, Electric Power Systems Research,.vol.81,pp. 43–50, 2011.

[15] Ollervides.j, Santibáñez..M, Lama.A, Dzul.A,, Aplicación de Control Borroso a un Sistema de Suspensión Magnética: Comparación Experimental, Revista Iberoamericana de Automática e Informática industrial,vol. 7,no3,pp.1697–7912,

[16] M. farhat, L. Sbita, ''ANFIS controlled solar pumping system, '' i-manager's Journal on Electronics Engineering, Vol. 2, no. 2, march-march 2011

[17] S. Thiruvenkadam, A. N. Kumar, and A. Sakthivel, "Distribution feeder energy conservation by using hybrid Neuro-Fuzzy approach," I-manager's Journal on Electrical Engineering, Vol.1, no. 3, pp. 45-52, 2008.

[18] S. Sankar," Simulation and Application of ANN in Fuzzy logic System, " I-manager's Journal on Future Engineering and Technology, Vol. 6, No. 1.pp 44-50, 2010.

[19] M. Alata, M. A. Al-Nimr, "Developing a multipurpose sun tracking system using fuzzy control, Energy Conversion and Management: 46, pp. 1229-1245,2005.

[20] C. T. Chi, S.A. Yin, Speed measurement of a general DC brushed motorbased on sensorless method,IEEE Conference on Power & Energy IPEC, 2012

[21] K. Niruba, S.Boopathi, Advanced power window motor using permanent Magnet DC motor, IEEE Power and Energy Systems Conference: Towards Sustainable Energy, 2014

[22] A. Hamidat, B. Benyoucef, M.T. Boukadoum,"New approach to determine the performances of the photovoltaic pumping system," Revue des Energies Renouvelables ICRESD, Tlemcen, pp. 101-107, 2007.

[23] M. Asim, A.Tariq & A. Sarwar, "Simulation and Analysis of a Directly Coupled Solar PV Based Water Pumping System," Journal on Electrical Engineering, Vol.2, no.3, 2009

IntechOpen